



저작자표시 2.0 대한민국

이용자는 아래의 조건을 따르는 경우에 한하여 자유롭게

- 이 저작물을 복제, 배포, 전송, 전시, 공연 및 방송할 수 있습니다.
- 이차적 저작물을 작성할 수 있습니다.
- 이 저작물을 영리 목적으로 이용할 수 있습니다.

다음과 같은 조건을 따라야 합니다:



저작자표시. 귀하는 원저작자를 표시하여야 합니다.

- 귀하는, 이 저작물의 재이용이나 배포의 경우, 이 저작물에 적용된 이용허락조건을 명확하게 나타내어야 합니다.
- 저작권자로부터 별도의 허가를 받으면 이러한 조건들은 적용되지 않습니다.

저작권법에 따른 이용자의 권리는 위의 내용에 의하여 영향을 받지 않습니다.

이것은 [이용허락규약\(Legal Code\)](#)을 이해하기 쉽게 요약한 것입니다.

[Disclaimer](#) 

공학 석사 학위논문

**Phase Error Correction for a Robust Surface
Reflectivity-Invariant 3-D Scanning**

표면 반사도에 강건한 3차원 스캔을 위한

Phase Error 보정 연구

2018 년 08 월

서울대학교 대학원

기계항공공학부

김정희

Abstract

Phase Error Correction for a Robust Surface Reflectivity-Invariant 3-D Scanning

Jeong Hee Kim

Department of Mechanical Engineering

The Graduate School

Seoul National University

A phase error correction method is proposed to produce an absolute phase with robustness, specifically by utilizing phases generated at high frequency. The proposed algorithm integrates spatiotemporal phase unwrapping into a 3D scanning system by transmitting a unique phase signal through its projector and capturing the patterned surface of an object through cameras at two different perspectives. By projecting multiple fringe patterns on the object surface, the algorithm obtains and analyzes spatiotemporal information of an object. The algorithm looks for phases containing errors and rectifies them by redirecting the misled fringe orders to the correct values. As the algorithm corrects errors for both images obtained from the left and right cameras, it processes and reconstructs them into a 3-D model. The suggested method allows for 3-D scanning objects with varied surface qualities. In doing so, neither of the scanning setup nor the algorithm requires modification with respect to the object to be scanned. Also, the object does not need to undergo any surface treatment to put it in a favorable condition for scanning. With the error-

correction algorithm, the noise in an image caused by a phase error can be effectively adjusted, thus yielding a robust 3-D scanning result.

Key Words : 3D scanning, Temporal phase unwrapping, Fringe order correction, Phase error correction

Student Number : 2016-22328

Contents

ABSTRACT	I
LIST OF TABLES.....	IV
LIST OF FIGURE.....	V
LIST OF SYMBOLS.....	VII
CHAPTER 1. INTRODUCTION.....	1
1.1. OVERVIEW OF 3-D SCANNING SYSTEM.....	1
1.1.1. <i>Stereo Camera Setup</i>	1
1.1.2. <i>Structured Fringe Pattern</i>	4
1.2. MOTIVATION AND OBJECTIVE	5
1.2.1. <i>Dynamic Reflection Behaviors Based on Surface</i>	6
CHAPTER 2. RELATED WORKS	10
CHAPTER 3. PRINCIPLES OF PHASE UNWRAPPING	12
3.1. OVERVIEW OF THE ALGORITHM.....	12
3.1.1. <i>Temporal Phase Unwrapping Algorithm: Number-Theoretical Approach</i>	13
3.1.2. <i>Selection of Three Spatial Frequencies</i>	20
CHAPTER 4. PHASE ERROR CORRECTION.....	23
4.1. OVERVIEW OF THE ERROR CORRECTION.....	23
4.1.1. <i>True Value Filtering Procedure</i>	24
4.1.2. <i>Error Correction Based on Filtered True Value</i>	28
CHAPTER 5. RESULTS	31
5.1. EXPERIMENTAL RESULTS	31
5.1.1. <i>Plastic object: 3-D printed figurine</i>	33
5.1.2. <i>Metallic object: aluminum tin cover</i>	35
5.1.3. <i>Multi-material object: electrical connector</i>	37
5.2. DATA ANALYSIS ON RESULTS	39
CHAPTER 6. CONCLUSION.....	42
REFERENCES	43
초 록.....	47

List of Tables

Table 3-1. The fringe order with respect to the range of an absolute phase	17
Table 3-2. The LUT for wrapped phases generated at frequency = 3, 4, and 5 ...	18
Table 5-1. 3-D reconstructed results for the scanned objects	39-41
Table 5-2. Experimental results comparison	41

List of Figure

Figure 1-1. Epipolar geometry	2
Figure 1-2. Image rectification	3
Figure 1-3. Calculation of corresponding points	3
Figure 1-4. (a) A gray code pattern and (b) a phase-shifted pattern	4
Figure 1-5. Reflection of light at a plane surface	6
Figure 1-6. (a) Specular reflection behavior and (b) diffuse reflection behavior	8
Figure 3-1. The relationship between a wrapped phase and unwrapped phase with respect to a fringe order	12
Figure 3-2. The relationship between an absolute phase and the unwrapped phases generated at frequencies of 3, 4, and 5	14
Figure 3-3. The fringe order values for unwrapped phases generated at frequencies of 3, 4, and 5	16
Figure 3-4. The structured fringe patterns generated at (a) $f = 71$, (b) $f = 100$, and (c) $f = 113$	21
Figure 4-1. The fringe order before and after the application of median filtering	25
Figure 4-2. (a) Original unwrapped phase map, (b) median filtered unwrapped phase map, and (c) standard deviation filtered unwrapped phase map	27
Figure 4-3. Key value distribution map	28
Figure 5-1. Objects tested for 3-D scanning (a) a plastic object, (b) a metallic object, and (c) a multi-material object	32
Figure 5-2. (a-b) Left unwrapped phase maps, (c-d) right unwrapped phase maps, and (e-f) disparity maps for a 3-D printed figurine; (a, c, e) without error correction and (b, d, f) with error correction applied	34
Figure 5-3. (a-b) Left unwrapped phase maps, (c-d) right unwrapped phase maps, and (e-f) disparity maps for an aluminum tin cover; (a, c, e) without error correction and (b, d, f) with error correction applied	36

Figure 5-4. (a-b) Left unwrapped phase maps, (c-d) right unwrapped phase maps, and (e-f) disparity maps for an electrical connector; (a, c, e) without error correction and (b, d, f) with error correction applied 38

List of Symbols

Φ	Unwrapped Phase
Ψ	Key Value
φ	Wrapped Phase
ϕ	Shifted Value
m	Fringe Order
f	Frequency
I	Intensity
i	i^{th} Phase

CHAPTER 1. Introduction

1.1. Overview of 3-D Scanning System

The acquisition of 3-dimensional (3-D) information is the primary algorithm for a scanning system. The 3-D point cloud is made up of the fundamental data that possess the features and directional information of a scanned object. The algorithm obtains 3-D scanned data of an object by processing and analyzing multiple digital images of an object. As the structured fringe pattern is projected from a projector, cameras capture an image of surface with the pattern from various perspectives. In the following subsections, the stereo camera setup and structured fringe pattern are explained in detail.

1.1.1. Stereo Camera Setup

The 3-D scanning system includes one projector and two cameras positioned at different angles with respect to the object. The cameras perceive the object from two different perspectives capture their respective images at the same time. Despite the difference in perspective, both images share certain features of the object. The correspondence points can be obtained based on the shared features that are present in both images. The correspondence points serve as keys to calculate a disparity map. By comparing two images with respect to the correspondence points, the disparity map - encoded with relative depth information - can be obtained. As the disparity map is calculated, the map gives insight into the scene depth at every corresponding pixel location in the images.

In the process of obtaining the disparity map, triangulation is utilized. Epipolar geometry primarily applies triangulation. As shown in Figure 1-1, epipolar geometry presents the relationship between two 2-D images by projecting 2-D

coordinates onto a 3-D domain. Based on the projection, the geometric relation between the two images is derived, and the correspondence points can be found where the projection lines from each image intersect.

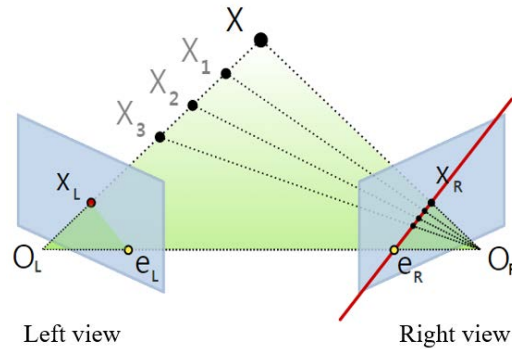


Figure 1-1. Epipolar geometry [20]

For example, point X in the 3-D domain is projected as point X_L to the 2-D left view with an image center at O_L in Figure 1-1. By utilizing the epipolar geometry, the corresponding point in the 2-D right view can be easily determined by inspecting pixels lying only on the red line. The red line in the right view is also known as the epipolar line. The 3-D point, X , must reside on the straight line stretched from points O_L and X_L . Because the straight line drawn by the points in the left view matches the epipolar line in the right 2D domain, the corresponding point can be found.

In addition to utilizing epipolar geometry, image rectification is applied to the system to find corresponding pixel between images obtained from two cameras. Applying image rectification to the system simplifies the image and locates the epipolar line with respect to the corresponding image obtained by the other camera. As shown in Figure 1-2, image rectification aligns the two images captured from different perspectives for an identical object. Because the images now lie on the same image plane, the epipolar line can be found on the same line in both images along the horizontal direction after applying the image rectification.

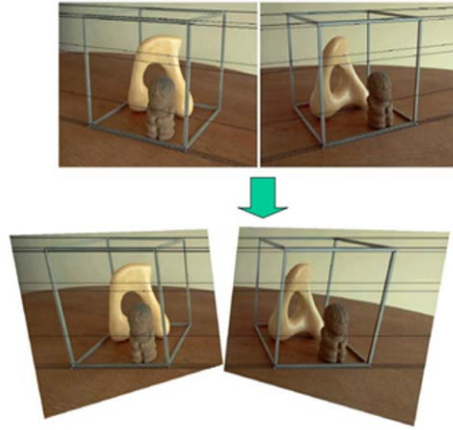


Figure 1-2. Image rectification [21]

With the corresponding pixels found from the left and right images, the corresponding 3-D coordinate can be obtained using triangulation. In Figure 1-3, calculating the 3-D coordinate of a point is described in detail.

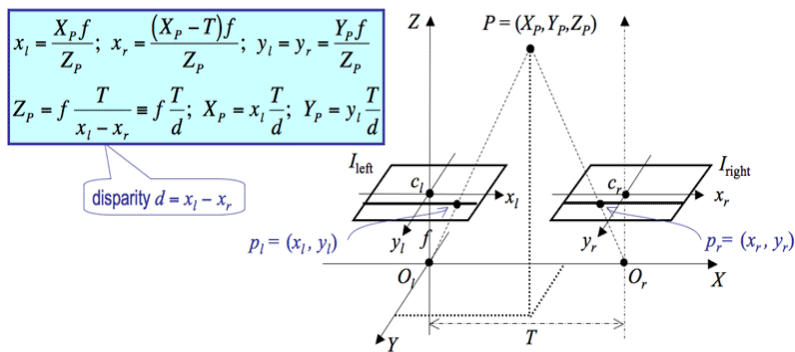


Figure 1-3. Calculation of corresponding points [22]

Exact, corresponding 2-D pixels from the left and right images are required for obtaining an accurate point in a 3-D domain. A signal is added to the stereo camera setup to guarantee the accuracy of correspondence points. In this research, structured light, as a signal, is projected to the object. In the following subsection, the structured light is examined in detail with respect to its generation, projection, and analysis methods.

1.1.2. Structured Fringe Pattern

To acquire the features of the scanned object, the structured fringe patterns are generated and projected to the object from a projector. The fringe pattern used in the projection is a phase-shifted pattern, which contains phase information.

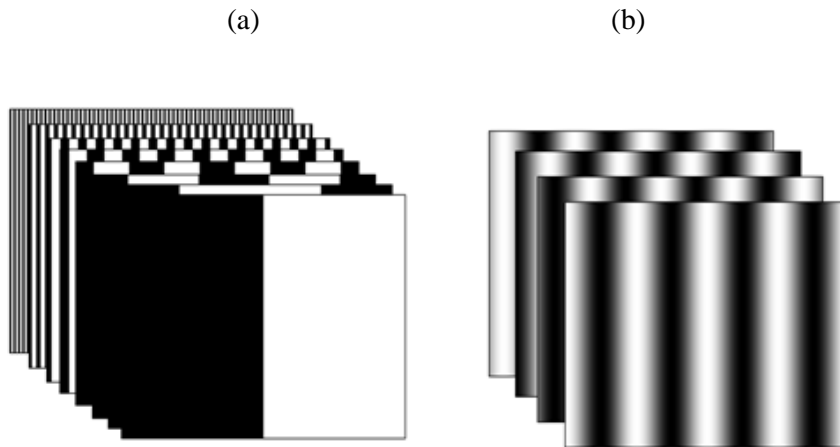


Figure 1-4. (a) A gray code pattern and (b) a phase-shifted pattern

Two types of fringe pattern are generally utilized for the pattern generation: a gray code pattern and a phase-shifted pattern, as shown in Figure 1-4 (a) and (b), respectively. A gray code pattern, also known as a binary pattern, obtains the feature information of an object by halving the projection space. As the first pattern halved the projection space, the second pattern halved them again. This creates a pattern with four regions, and the space is sequentially halved in the same manner. However, this method is not desirable because phase information is lost on the boundary between the two regions. Additionally, the scanned quality of the surface feature highly depends on the number of patterns projected on the object. However, a phase-shifted pattern, generated at a particular frequency, contains phase information. As cameras capture a patterned image of an object, the phase information projected on the surface can be acquired. A unique phase value is assigned to every pixel in the

captured image, which facilitates an accurate analysis of the surface feature. The phase information can be analyzed by processing signal intensity (I) of pixels at location (x, y) in an i^{th} image, as seen in Equation 1-1. The phase information includes the wrapped phase and shifted value, represented as φ and ϕ^i , respectively. The signal intensity varies depending on camera properties, which appear in the equation as: A – ambient light intensity; B – reflectivity.

$$I^i(x, y) = A(x, y) + B(x, y) \cdot \cos(\varphi(x, y) + \phi^i) \quad (1-1)$$

A temporal analysis can be conducted on the signal intensity by shifting an identical fringe pattern into several steps. In general, the pattern is shifted into 3, 4, or 6 steps. The steps define the number of intervals in one period of a fringe pattern. In this research, a 6-step phase shifting is applied to the fringe pattern, which is calculated as Equation 1-2.

$$\tan\varphi = -\frac{\sqrt{3}(I_2+I_3-I_5-I_6)}{2I_1+I_2-I_3-2I_4-I_5+I_6} \quad (1-2)$$

According to Equation 1-2, the wrapped phase (φ) is obtained by taking the inverse tangent on both sides, which is bounded between $-\pi$ and $+\pi$. The wrapped phases then undergo an unwrapping process, explained in the following chapter, for acquiring correspondence points in images obtained from the stereo camera.

1.2. Motivation and Objective

The objective of the research is for a system to guarantee a robust 3-D scan. The goal can be achieved by implementing a spatiotemporal, quality-guided phase error correction into the algorithm.

Most 3-D scanners require frequent calibration before scanning an object to robustly obtain 3-D point information in the constantly changing conditions of the scanning environment. If an object to be scanned is replaced and the replacement has different surface specifications, the scanner needs to start anew for the calibration procedure. For some scanners, a limited type of objects can only be scanned, such that a dental scanner is specifically designed to scan dental casts.

This type of repetition of a procedure or a limitation on scanning an item is obligatory for a scanner to prevent the propagation of a phase error. The phase error is one of the major components that affects the quality of the 3-D scanning results. For this reason, suppressing or eliminating the phase error in the obtained 3-D information is the key to 3-D reconstruction. In this research, robust 3-D scanning of various objects is accommodated by applying a spatiotemporal, quality-guided phase error correction instead of repeating the calibration.

1.2.1. Dynamic Reflection Behaviors Based on Surface

The law of reflection must be understood prior to a 3-D scanning process. In general, the reflection of light at a plane surface is described in Figure 1-5.

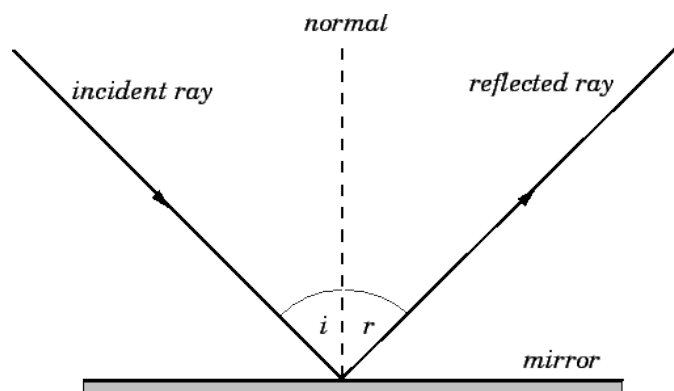


Figure 1-5. Reflection of light at a plane surface [23]

For light to be reflected as shown in Figure 1-5, it is assumed that the object has a planar, smooth surface. This surface theoretically does not absorb or transmit light. For such a complete reflection to occur, the wavelength of the incident light must be several times greater than the average surface profile height is. However, the spectrum of visible light rarely satisfies such a condition, and light does not behave exactly as the law of reflection does when it interacts with a surface. In fact, the behavior of light highly depends on the medium, surface roughness, and subsurface reflectivity.

The behavior of light is categorized as specular reflection and diffuse reflection. If light interacts with a polished surface and diffuse medium, specular reflections appear. Specular reflection generally obeys the law of reflection, as shown in Figure 1-6 (a). In specular reflection, a dominant, directional component is reflected by the surface in accordance with the incident ray. However, diffuse reflection occurs if light is projected on an object with a reflective subsurface and rough surface. As shown in Figure 1-6 (b), light is uniformly reflected around the surface in every direction without any noticeable component of specific directionality in this instance.

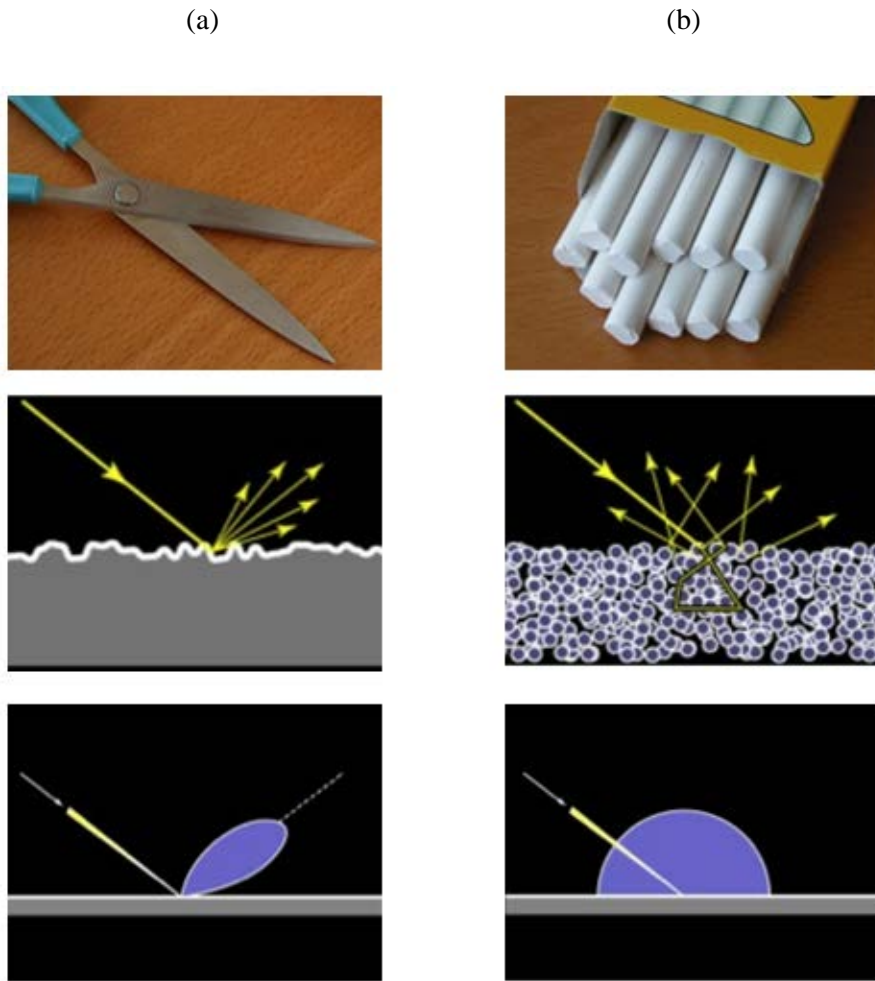


Figure 1-6. (a) Specular reflection behavior and (b) diffuse reflection behavior

Such a difference in reflection behavior based on the medium affects the quality of 3-D scanning results. If the object of interest has a rough and matte surface, such as chalk, the fringe pattern projected on the surface would have diffuse reflection. With diffuse reflection behavior, a camera can capture the patterned image of an object from any perspective. Because the intensity of light reflected from the surface is uniform, the intensity of the captured pattern is consistent regardless of the angle of observation. However, if the object to be scanned has a glossy and smooth surface, such as scissors, specular reflection would occur as the pattern is projected. In this case, the intensity of the reflected light would vary depending on

the angle of camera observation. A relatively high intensity of light would be observed around the angle of reflection, while the light would fade away as it is drifted off from the angle of reflection. Because of the variation in light intensity depending on the location of the camera, acquiring the correct data for accurate 3-D scanning of an object becomes challenging.

CHAPTER 2. Related Works

A fringe projection profilometry has been extensively studied and conducted for a 3-D scan [1, 4-6, 12-13]. Various attempts have been made to increase the robustness of the 3-D scanning by implementing phase shifting and projecting multiple patterns [8-10, 14-15, 17]. However, such approaches were limited to an extent that low frequencies are utilized for the pattern generation. Despite low resolution images as scanned results, low frequencies were utilized to generate a fringe pattern because the phase errors could be moderately controlled during the data processing of the 3-D points.

As the demand for enhancement in scanned results increases, approaches to eliminate and suppress noises due to phase errors were practiced. One of such approaches was the construction of a lookup table (LUT) [7-9, 11]. By referencing to the LUT, Zhong, *et al.* and Ding, *et al.* sought to estimate an accurate fringe order and unwrapped phase. However, the accuracy of the estimation was not high enough to reconstruct a complete 3-D scanned model. Also, a reliability-based phase unwrapping and quality-based phase unwrapping methods were introduced [6, 16]. These methods unwrapped the wrapped phases by qualifying or assigning values, such as reliability and quality, to every pixel in the captured 2-D image. However, such methods required unnecessary, additional calculations. The extra calculations not only delayed the overall 3-D scanning process, but also occupied memory space for conducting calculations and storing the calculated results.

Additionally, one of the major challenges to conduct 3-D scanning is scanning objects with various surface conditions. While matte, opaque surfaces are favorable for the scanning, glossy and reflective surfaces are difficult to obtain accurate feature information because of specular reflection [19]. To deal with such

limitations, additional coating or matte powder was pervasively applied to the objects with glossy surfaces and rough edges [2-3, 18]. The treatments on the object surface could make the object in a more favorable condition for scanning by controlling specular reflection to behave as diffuse reflection. In doing so, object could be observed from any perspective, regardless of the position of a camera. However, such surface treatments do not satisfy the purpose of non-contact and non-destructive scanning of the fringe projection profilometry, by artificially transforming the object.

This research intends to resolve such challenges in 3-D scanning through an algorithmic approach. This study engages in error correction of fringe orders without corrupting object surfaces. The correction is made based on a priori information of pixels, simplifying the calculation procedure compared to the previous studies.

CHAPTER 3. Principles of Phase Unwrapping

3.1. Overview of the Algorithm

The fundamental relationship between an unwrapped phase (Φ) and wrapped phase (φ) is shown in Equation 3-1, where the range of the unwrapped phase lies within $-f_i\pi < \Phi_i < f_i\pi$.

$$\Phi_i = 2\pi \cdot m_i + \varphi_i \quad (3-1)$$

The relationship is also described in Figure 3-1 - for example, the pattern is generated at a frequency of 3.

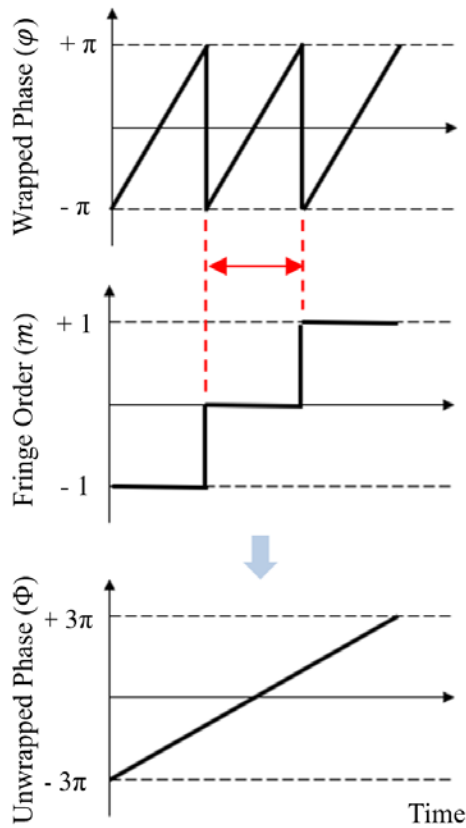


Figure 3-1. The relationship between a wrapped phase and unwrapped phase with respect to a fringe order

To implement a 3D scanning, an originally wrapped phase has to undergo an unwrapping process and obtain an unwrapped phase. The unwrapping process requires several calculations on wrapped phases, which are described as follows.

3.1.1. Temporal Phase Unwrapping Algorithm: Number-Theoretical Approach

A temporal phase unwrapping method utilizes at least two phases in the generation of a phase pattern. By utilizing multiple phases, the method intends to eliminate ambiguity that appeared in a single phase and determines the fringe order of each phase by examining the relationship between each pattern. Among three approaches to conduct temporal phase unwrapping – multi-frequency, multi-wavelength, and number-theoretical – to conduct temporal phase unwrapping, number-theoretical approach is utilized for this research because it aptly uncovers phase information within the fringe pattern generated at a diverse frequency range and works robustly at phase jumps [6].

In this research, the phase patterns are generated at three frequencies. The selection of the frequencies is explained in detail in the following subsection. With the selected frequencies, three time-shifted phase patterns are generated as Equation 3-2, each with a different unwrapped phase range based on the frequency.

$$\begin{cases} \Phi_1 = 2\pi \cdot m_1 + \varphi_1 \\ \Phi_2 = 2\pi \cdot m_2 + \varphi_2 \\ \Phi_3 = 2\pi \cdot m_3 + \varphi_3 \end{cases} \quad (3-2)$$

The relationship between the unwrapped phases can be defined by transforming each phase into an absolute phase, as in Equation 3-3.

$$\Phi_{abs} = \frac{\Phi_1}{f_1} = \frac{\Phi_2}{f_2} = \frac{\Phi_3}{f_3}$$

, where $-\pi \leq \Phi_{abs} \leq \pi$ (3-3)

For example, the relationship between an absolute phase and the other unwrapped phases generated at frequencies of 3, 4, and 5 can be described in Figure 3-2.

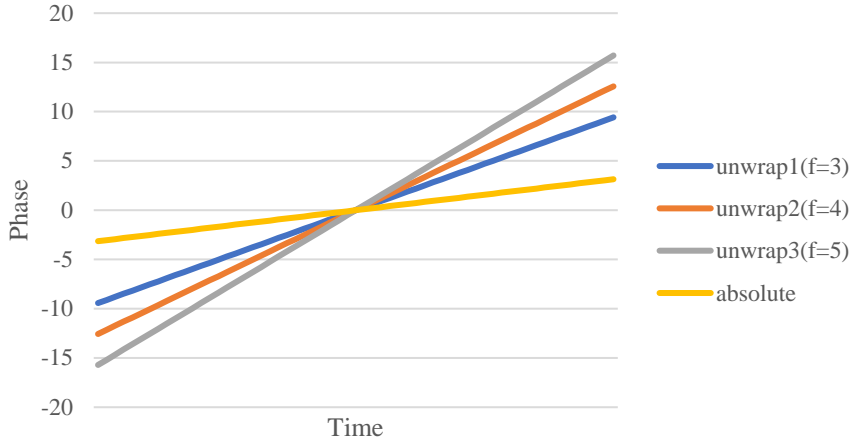


Figure 3-2. The relationship between an absolute phase and the unwrapped phases generated at frequencies of 3, 4, and 5

Based on the relationship between an absolute phase and the unwrapped phases in Equation 3-3, an unwrapped phase can be compared to another, as defined in Equation 3-4.

$$\begin{cases} f_2 \cdot \Phi_1 = f_1 \cdot \Phi_2 \\ f_3 \cdot \Phi_2 = f_2 \cdot \Phi_3 \\ f_1 \cdot \Phi_3 = f_3 \cdot \Phi_1 \end{cases} \quad (3-4)$$

By replacing the unwrapped phase in Equation 3-4 with the corresponding relationship in Equation 3-2, each phase relationship can be described as a wrapped phase in Equation 3-5.

$$\begin{cases} f_2 \cdot (2\pi \cdot m_1 + \varphi_1) = f_1 \cdot (2\pi \cdot m_2 + \varphi_2) \\ f_3 \cdot (2\pi \cdot m_2 + \varphi_2) = f_2 \cdot (2\pi \cdot m_3 + \varphi_3) \\ f_1 \cdot (2\pi \cdot m_3 + \varphi_3) = f_3 \cdot (2\pi \cdot m_1 + \varphi_1) \end{cases} \quad (3-5)$$

By separating known values to the left and unknown values to the right side of the Equation 3-5, a key value (Ψ) can be defined as Equation 3-6.

$$\begin{cases} \frac{f_2 \cdot \varphi_1 - f_1 \cdot \varphi_2}{2\pi} = f_1 \cdot m_2 - f_2 \cdot m_1 \\ \frac{f_3 \cdot \varphi_2 - f_2 \cdot \varphi_3}{2\pi} = f_2 \cdot m_3 - f_3 \cdot m_2 \\ \frac{f_1 \cdot \varphi_3 - f_3 \cdot \varphi_1}{2\pi} = f_3 \cdot m_1 - f_1 \cdot m_3 \end{cases} \quad (3-6)$$

The left key value, which can be calculated from the obtained phase pattern, is then redirected to the corresponding fringe order by referencing an LUT. An LUT is a table displaying a relationship between a key value combination (Ψ_1, Ψ_2, Ψ_3) and the corresponding fringe order combination (m_1, m_2, m_3). Using an LUT allows the fringe order for a phase pattern to be determined efficiently. While the left key value is computable, the right key is unclear because of the fringe order.

Although it is difficult to obtain the fringe order directly from Equation 3-6, its value can be estimated by its characteristics. The fringe order gradually increases/decreases from the center with the fringe order value of 0, as shown in Figure 3-3. The range of fringe order is estimated as $-\lfloor \frac{f_i}{2} \rfloor \leq m_i \leq \lfloor \frac{f_i}{2} \rfloor$, where $\lfloor \cdot \rfloor$ stands for a maximum integer less than or equal to the value in the bracket.

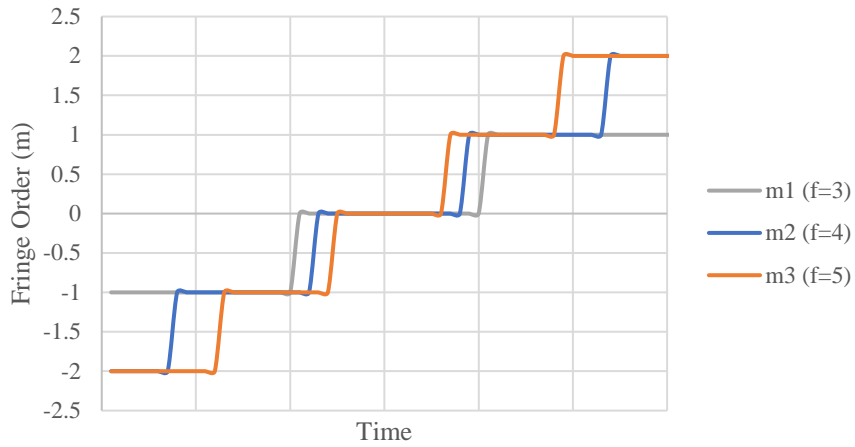


Figure 3-3. The fringe order values for unwrapped phases generated at frequencies of 3, 4, and 5

The stepwise characteristics of the fringe order allow an estimate of the fringe order value with respect to the corresponding unwrapped phase range, as shown in Table 3-1 ($i= 1, 2, 3$).

Table 3-1. The fringe order with respect to the range of an absolute phase

Fringe Order (m_i)	Range of Absolute Phase (Φ_{abs})
$\left\lfloor \frac{f_i}{2} \right\rfloor$	$\frac{\pi[f_i - (f_i \bmod 2 + 1)]}{f_i} \leq \Phi_{abs} < \pi$
...	...
1	$\frac{\pi}{f_i} \leq \Phi_{abs} < \frac{3\pi}{f_i}$
0	$-\frac{\pi}{f_i} < \Phi_{abs} < \frac{\pi}{f_i}$
-1	$-\frac{3\pi}{f_i} \leq \Phi_{abs} < -\frac{\pi}{f_i}$
...	...
$-\left\lfloor \frac{f_i}{2} \right\rfloor$	$-\pi < \Phi_{abs} \leq -\frac{\pi[f_i - (f_i \bmod 2 + 1)]}{f_i}$

The LUT can be generated by combining the fringe order estimation, found in Table 3-1, and the right key, calculated in Equation 3-6. With the LUT, the left key values, which are calculated with the obtained wrapped phases, can be directed to their corresponding fringe order combinations. For example, the LUT for frequencies at 3,4 and 5 can be generated as Table 3-2.

Table 3-2. The LUT for wrapped phases generated at frequency = 3, 4, and 5

Absolute Phase (Φ_{abs})	Fringe Order (m_1, m_2, m_3)	Left Key (Ψ_i)		
		$\frac{f_2 \cdot \varphi_1}{2\pi}$	$\frac{f_3 \cdot \varphi_2}{2\pi}$	$\frac{f_1 \cdot \varphi_3}{2\pi}$
		$-\frac{f_1 \cdot \varphi_2}{2\pi}$	$-\frac{f_2 \cdot \varphi_3}{2\pi}$	$-\frac{f_3 \cdot \varphi_1}{2\pi}$
$\frac{3}{4}\pi \leq \Phi_{abs} < \pi$	-1, -2, -2	-2	2	1
$\frac{3}{5}\pi \leq \Phi_{abs} < \frac{3}{4}\pi$	-1, -1, -2	1	-3	1
$\frac{1}{3}\pi \leq \Phi_{abs} < \frac{3}{5}\pi$	-1, -1, -1	1	1	-2
$\frac{1}{4}\pi \leq \Phi_{abs} < \frac{1}{3}\pi$	0, -1, -1	-3	1	3
$\frac{1}{5}\pi \leq \Phi_{abs} < \frac{1}{4}\pi$	0, 0, -1	0	-4	3
$-\frac{1}{5}\pi < \Phi_{abs} < \frac{1}{5}\pi$	0, 0, 0	0	0	0
$-\frac{1}{4}\pi < \Phi_{abs} \leq -\frac{1}{5}\pi$	0, 0, 1	0	4	-3
$-\frac{1}{3}\pi < \Phi_{abs} \leq -\frac{1}{4}\pi$	0, 1, 1	3	-1	-3
$-\frac{3}{5}\pi < \Phi_{abs} \leq -\frac{1}{3}\pi$	1, 1, 1	-1	-1	2
$-\frac{3}{4}\pi < \Phi_{abs} \leq -\frac{3}{5}\pi$	1, 1, 2	-1	3	-1
$-\pi < \Phi_{abs} \leq -\frac{3}{4}\pi$	1, 2, 2	2	-2	-1

As the left key values are calculated from Equation 3-6, the fringe orders for each phase are matched by utilizing the LUT generated as Table 3-2. Because the corresponding fringe orders are found by using the LUT, the unwrapped phase can finally be estimated in Equation 3-1.

However, the unwrapping process holds a weakness with patterns generated at high frequencies because the phase errors - if they exist - are propagated as they are unwrapped. Because phase errors randomly reside within the wrapped phase, the errors are amplified when they interact with high frequency patterns, as shown in Equation 3-7.

$$\Psi_{with\ error} = \begin{bmatrix} \frac{f_2 \cdot (\varphi_1 + \varepsilon_1) - f_1 \cdot (\varphi_2 + \varepsilon_2)}{2\pi} \\ \frac{f_3 \cdot (\varphi_2 + \varepsilon_2) - f_2 \cdot (\varphi_3 + \varepsilon_3)}{2\pi} \\ \frac{f_1 \cdot (\varphi_3 + \varepsilon_3) - f_3 \cdot (\varphi_1 + \varepsilon_1)}{2\pi} \end{bmatrix} = \begin{bmatrix} \frac{f_2 \cdot \varphi_1 - f_1 \cdot \varphi_2}{2\pi} \\ \frac{f_3 \cdot \varphi_2 - f_2 \cdot \varphi_3}{2\pi} \\ \frac{f_1 \cdot \varphi_3 - f_3 \cdot \varphi_1}{2\pi} \end{bmatrix} - \begin{bmatrix} \frac{f_2 \cdot \varepsilon_1 - f_1 \cdot \varepsilon_2}{2\pi} \\ \frac{f_3 \cdot \varepsilon_2 - f_2 \cdot \varepsilon_3}{2\pi} \\ \frac{f_1 \cdot \varepsilon_3 - f_3 \cdot \varepsilon_1}{2\pi} \end{bmatrix} \quad (3-7)$$

Confirmed by Equation 3-7, the phase errors influence obtaining a key value and affect the process of finding the corresponding fringe order by referencing an LUT. Thus, the obtained fringe order would lead an unwrapped phase to the wrong result.

To prevent the corruption of phase errors in the process of phase unwrapping, an error correction algorithm was designed and applied to this research. By applying the correction algorithm, the phase - influenced by phase errors - was guided to the most appropriate key value and fringe order so that the phase is correctly unwrapped. In the next section, the phase error correction method and its application are discussed in detail.

3.1.2. Selection of Three Spatial Frequencies

Three different frequencies - $f_1 = 71$, $f_2 = 100$ and $f_3 = 113$ - were utilized to generate their respective structured fringe patterns. The generated patterns are shown in Figure 3-4. The frequencies were selected according to the frequency selection method suggested by Ding [9]. As proposed, the chosen frequency values do not have any common factor other than 1. Additionally, two from the selection are prime, odd numbers, and the other is an even number.

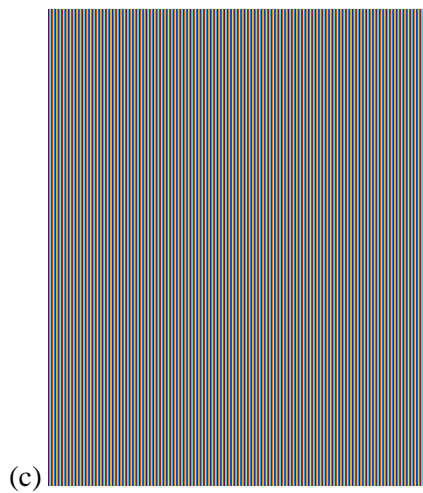
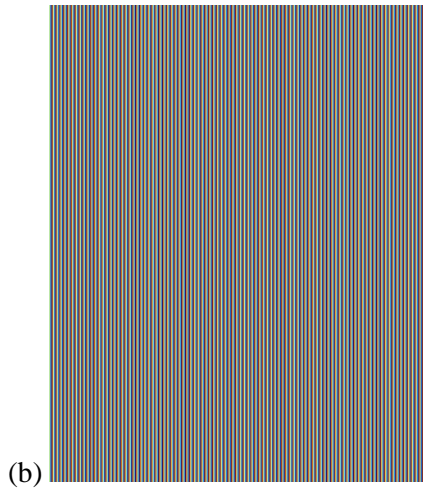
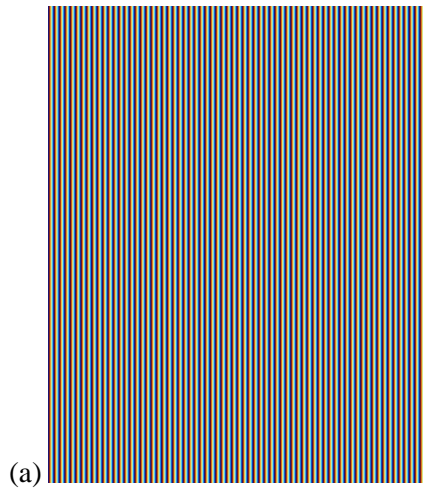


Figure 3-4. The structured fringe patterns generated at (a) $f_1 = 71$, (b) $f_2 = 100$, and

(c) $f_3 = 113$
21

In deciding frequency selection, high frequencies are considered so the influence of phase errors residing in the wrapped phase can be clearly observed. Although utilizing the high frequencies would yield a clear 3-D scanned result with a high resolution, previous studies on phase unwrapping avoided using it to generate a structured pattern because of the propagation of the phase error. In this study, phase errors interacting with high frequencies are corrected to the phases that are pertinent to their true values.

CHAPTER 4. Phase Error Correction

4.1. Overview of the Error Correction

In this study, the phase error correction algorithm is designed so a wrapped phase could be directed to the correct unwrapped phase. This research devised phase error correction algorithm and applied the algorithm into the general phase unwrapping procedure. The error correction algorithm is composed of two major steps: the acquisition of true fringe order and the propagation of the obtained true fringe order to the neighboring pixels.

To obtain the true fringe order from the captured 2-D image of a patterned object, the phase values for each pixel are inspected to discriminate between the correct and incorrect values. The true fringe order refers to the value, which is distinguished to have the correct fringe order. To obtain true fringe order from the captured 2D image of a patterned object, phase values for each pixel are inspected to discriminate between correct and incorrect values. To conduct the discrimination, several image-processing methods - median filtering and standard deviation filtering - were utilized. The application of the image processing methods to the 2D image of a patterned object would result in a filtered image that only the true regions would be remained, while the regions with incorrect fringe order values are nullified.

As the discrimination in the fringe order values was completed, the propagation was conducted based on the filtered true values. The propagation was conducted by comparing the unique pixel value to the value of the neighboring pixels. Through the propagation of true fringe order, the neighboring pixels, which initially had an incorrect fringe order due to phase errors, are redirected to the correct fringe order. In doing so, the pixels that were originally unwrapped to the incorrect values

become reliable. Thus, the error corrected 2-D image would be able to yield to 3-D reconstruction with robustness. In the following subsections, the error correction algorithm is described in detail.

4.1.1. True Value Filtering Procedure

In the process of phase unwrapping, phase errors are propagated from one step to the next. For this reason, noise usually corrupts an unwrapped phase map, and it is not possible to obtain correct 3-D scanned results. To prevent such a failure, pixels with noticeable phase errors should be omitted so they are processed to the next procedure. To do this, image-processing methods are applied to separate pixels with phase errors from pixels without phase errors in an image.

A median filter is applied in the fringe order calculation. Because of the stepwise characteristics of fringe order values, as shown in Figure 3-3, the median filtering effectively works on a step within the same level. The selection of the median filtering underlies an assumption that the correct values are dominant over the incorrect values in the range. If correct fringe orders are dominant, then the phase error affected ones can be filtered out and adjusted to the median value in the range. The median filtered image is resulted as shown in Figure 4-1. The median filtered results show that values, inconsistent with the rest of values within the same range, are corrected to more fitting values. Consequently, the stepwise feature of the fringe order is observed more clearly after median filtering is applied than the original fringe order function.

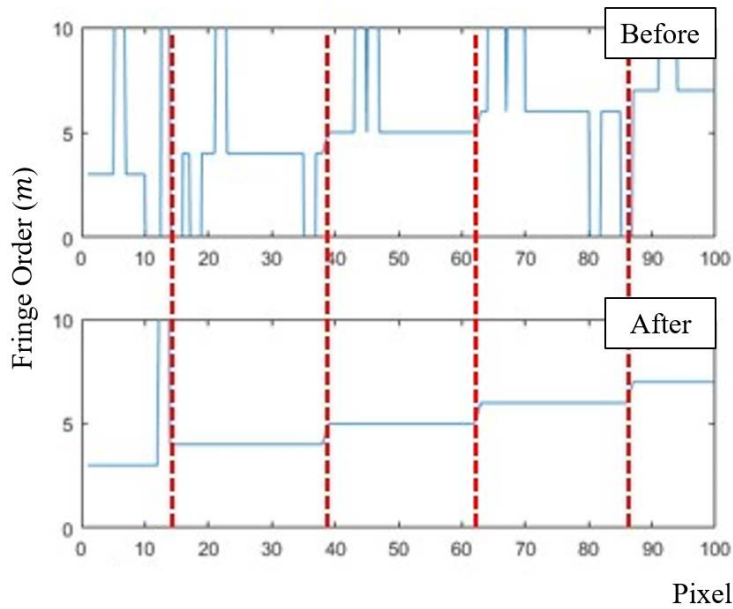


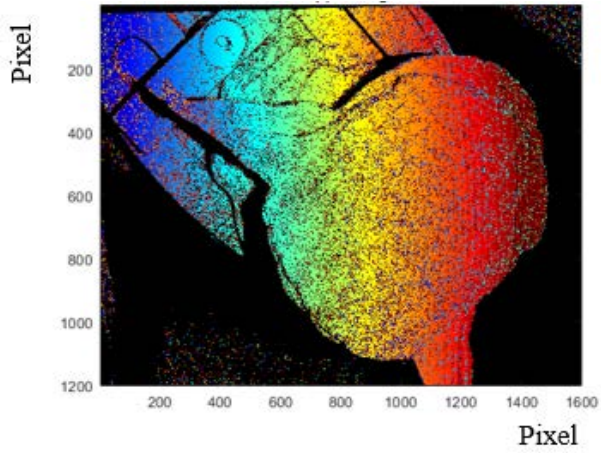
Figure 4-1. The fringe order before and after the application of median filtering

However, the correct fringe orders may be corrupted by incorrect values if the incorrect fringe orders are prevalent. In such a case, the correct fringe order would be replaced with an incorrect value after the filtering process. Additionally, the efficacy of the median filter is limited to the steps within the same value. Its performance on the boundary where fringe order jumps from one value to the other would be unreliable. Due to such a vulnerability of the median filter, an abnormal fringe order, observed at the boundary between fringe order values of 3 and 4 in Figure 4-1, is not rectified.

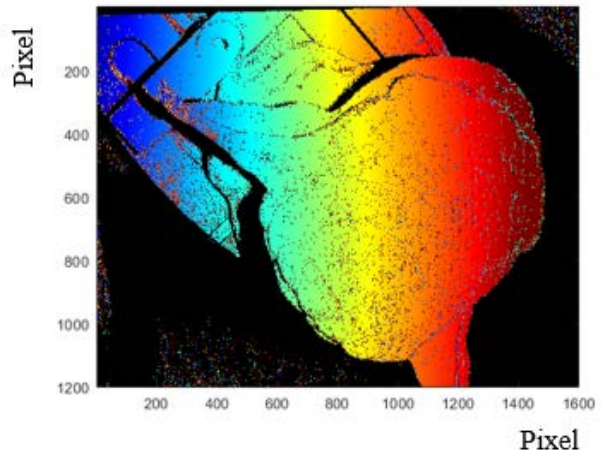
In addition to the median filter, a standard deviation filter is applied to the unwrapped phase generated with the median filtered fringe order to guarantee the discrimination between correct and incorrect values. Unlike fringe order values, the unwrapped phase is aligned continuously with values increasing or decreasing sequentially. Because it can correct the unwrapped phases which are inconsistent

with the neighboring unwrapped phases by comparing one another, the standard deviation filtering was selected for the error correction on unwrapped phase.

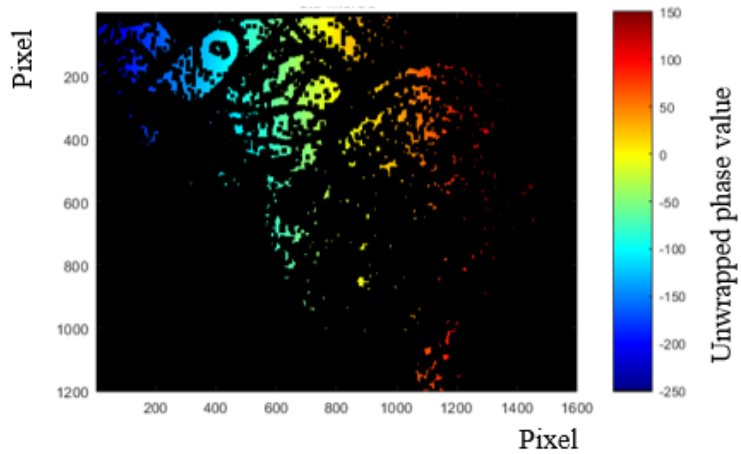
With standard deviation filtering, the scope of the neighborhood pixels can be managed from examination only on adjacent pixels to the extent all the unwrapped phase values that phase errors could affect are eliminated. Because the goal of the filtering procedure is to discriminate correct from incorrect values, the unwrapped phase is harshly assessed so that only correctly unwrapped phases are remained after applying the standard deviation filter.



(a)



(b)



(c)

Figure 4-2. (a) Original unwrapped phase map, (b) median filtered unwrapped phase map, and (c) standard deviation filtered unwrapped phase map

The filtered results are displayed in Figure 4-2. The color variation represents the unwrapped phase value. Based on the true values obtained after the filtering procedure, the error correction is made on the remaining values that have been filtered out. The process and application of error correction are discussed in detail in the following subsection.

4.1.2. Error Correction Based on Filtered True Value

Followed by the acquisition of the true unwrapped phases, the error correction is conducted based on the true values, beginning from the neighboring region.

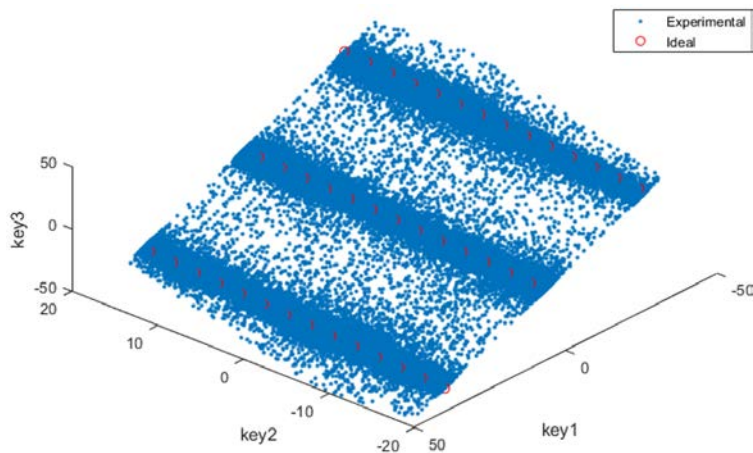


Figure 4-3. Key value distribution map

Phase errors hiding in wrapped phases disclose themselves as they interact with a high frequency, as described in Equation 3-7. For this reason, the calculated key values are found to be unreliable because they are drifted apart from the desired values. This aspect is observed in Figure 4-3, where the calculated key values from the experimental data and the desired, ideal data are represented in blue and red, respectively. In ideal conditions, the calculated key values should be positioned at

the corresponding key values. However, they are randomly distributed, which makes it difficult for them to be matched correctly with the fringe order combinations.

To prevent the propagation of phase errors, the error correction is suggested in this section. The correction is implemented based on the filtered true values by comparing key values and fringe orders of the true values to those of the adjacent incorrect values.

First, the search for candidates to conduct error correction begins from the neighboring incorrect pixels of the true value regions. As the neighboring incorrect pixels are selected, the key values of those pixels are examined. Because phase errors directly affect the key values, according to Equation 3-7, the key values were drifted away from the ideal keys that they were supposed to be. Thus, the error-affected key value should be redirected to an ideal key, which is assumed to be the original key value without the effect of phase errors.

The candidates for the corresponding ideal key for the error-affected key of an incorrect pixel are carefully selected based on the distance in the 3-D coordinates composed of three key values of the chosen pixel. The three closest ideal key values from the error-affected key of an incorrect pixel are selected as candidates. Instead of automatically switching to the nearest ideal key value, additional candidates are examined because the influence of phase error on the key value varies. If its influence were negligible, such that the observed key value is slightly drifted from the targeted ideal key, the error-affected key would still be within the range of the nearest ideal key. However, if the error were amplified as it reacts with the high frequency while calculating the key value, the incorrect key value would drift apart from the ideal key. In such a case, the nearest ideal key value may not be the intended key that is assumed to be unaffected by phase errors. Thus, three candidates of an ideal key value are investigated to increase the reliability of redirection of the key value.

The candidates of key values are then converted to their corresponding fringe order combinations. The fringe order combination of a neighboring true value pixel is obtained as well. To make a comparison, the distance between the fringe order combination of neighboring true value pixel and each candidate is measured. Among the three distances, the candidate with the shortest distance from the fringe order combination of true pixel is finally selected as the one for redirection. Such a comparison of the distance between fringe order combinations is possible because of the unique characteristic of fringe order that increases/decreases in an orderly manner. Theoretically, the fringe order of a pixel should be equal to the adjacent pixels if they are in the same fringe or have a difference of one fringe value if they are in different fringe.

As an ideal fringe order combination is finally determined for an incorrect pixel, its original incorrect fringe order is redirected to the newly selected fringe order combination. An identical procedure is iteratively executed for error correction. As a result, the true value regions expand, and the omitted regions after the filtering procedure are converted to the redirected, true fringe order.

CHAPTER 5. Results

5.1. Experimental Results

The phase error correction algorithm is applied to the initial phase unwrapping procedure for 3-D scanning. Consequently, the results are obtained and compared to those from the procedure without the proposed error correction method. To verify the performance of the proposed method, the error correction algorithm is tested on three objects with different materials: a plastic object, a metallic object, and a multi-material object, as shown in Figure 5-1. The experimental results for each object are introduced and discussed in the following subsections.



Figure 5-1. Objects tested for 3-D scanning (a) a plastic object, (b) a metallic object, and (c) a multi-material object – rubber and metal

5.1.1. Plastic object: 3-D printed figurine

A plastic object is tested for scanning, as shown in Figure 5-1(a). The surface incessantly has rough edges because of the characteristics of the fused deposition modeling, one of the popular types of 3-D printing. The uneven angles of rough edges cause the surface to glare, disturbing the cameras to accurately capture the features of an object.

The results from the general unwrapping procedure without the error correction and the procedure with the error correction applied are displayed in Figure 5-2. Figure 5-2(a) and (c) are the left and right unwrapped phase maps, respectively, which were generated utilizing the general unwrapping procedure. Figure 5-2(b) and (d) are the unwrapped phase maps that were generated with error correction algorithm in addition to the general unwrapping procedure.

Based on the obtained left and right unwrapped phase maps, disparity maps were generated as shown in Figure 5-2(e) and (f). By comparing the disparity maps from each method, the performance of the error correction is found to be highly reliable because noises are effectively eliminated after applying the error correction. While the disparity map without the error correction was corrupted by noise, the disparity map with the error correction clearly showed features of the scanned object. The facial features of the figurine, which are difficult to observe in Figure 5-2(e), can be found in Figure 5-2(f). Additionally, the boundary between the object and background is unclear in some regions of the map generated without the error correction.

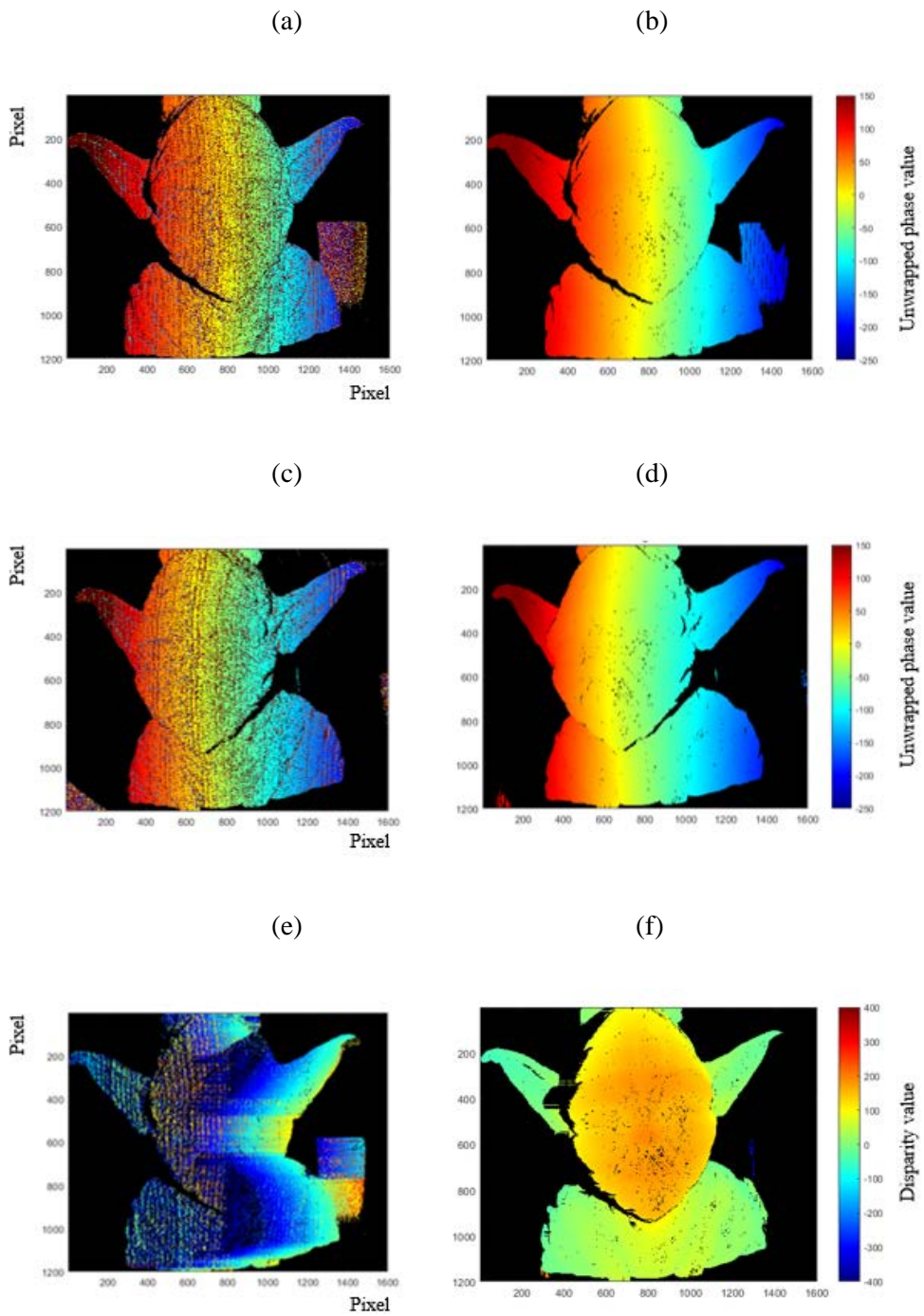


Figure 5-2. (a-b) Left unwrapped phase maps, (c-d) right unwrapped phase maps, and (e-f) disparity maps for a 3-D printed figurine; (a, c, e) without error correction and (b, d, f) with error correction applied

5.1.2. Metallic object: aluminum tin cover

An aluminum tin cover is tested as shown in Figure 5-1(b). Because metals have highly reflective surfaces, specular reflection occurs on the surface as the pattern is projected, making it difficult for cameras to capture patterned images of an object.

Regardless of the reflective characteristics of a metallic object, the performance of the error correction algorithm can be clearly observed in Figure 5-3. Utilizing the method without the error correction algorithm, the unwrapped phase maps from left and right cameras were generated as shown in Figure 5-3(a) and (c), respectively. Likewise, the unwrapped phase maps were generated by utilizing the method with the error correction as shown in Figure 5-3(b) and (d). While the maps generated by using the error correction is clear of noise on the object surface, the maps generated without the correction method is disrupted by noises. Also, background noises are much observed in the maps without the error correction applied.

Such traits found in the unwrapped phase maps can also be observed in the disparity maps generated based on them as shown in Figure 5-3(e) and (f). In Figure 5-3(e), the disparity map was generated without the error correction algorithm applied to the unwrapping procedure. It is difficult to observe an aluminum tin cover in this map because of the blurry boundaries between the scanned object and the background. Noises due to the phase errors also make it difficult to distinguish features on the object surface. On the other hand, the disparity map generated using the error correction clearly displays a scanned aluminum tin cover as shown in Figure 5-3(f). The object can be distinguished from the background, and the features on the surface can also be observed in this map.

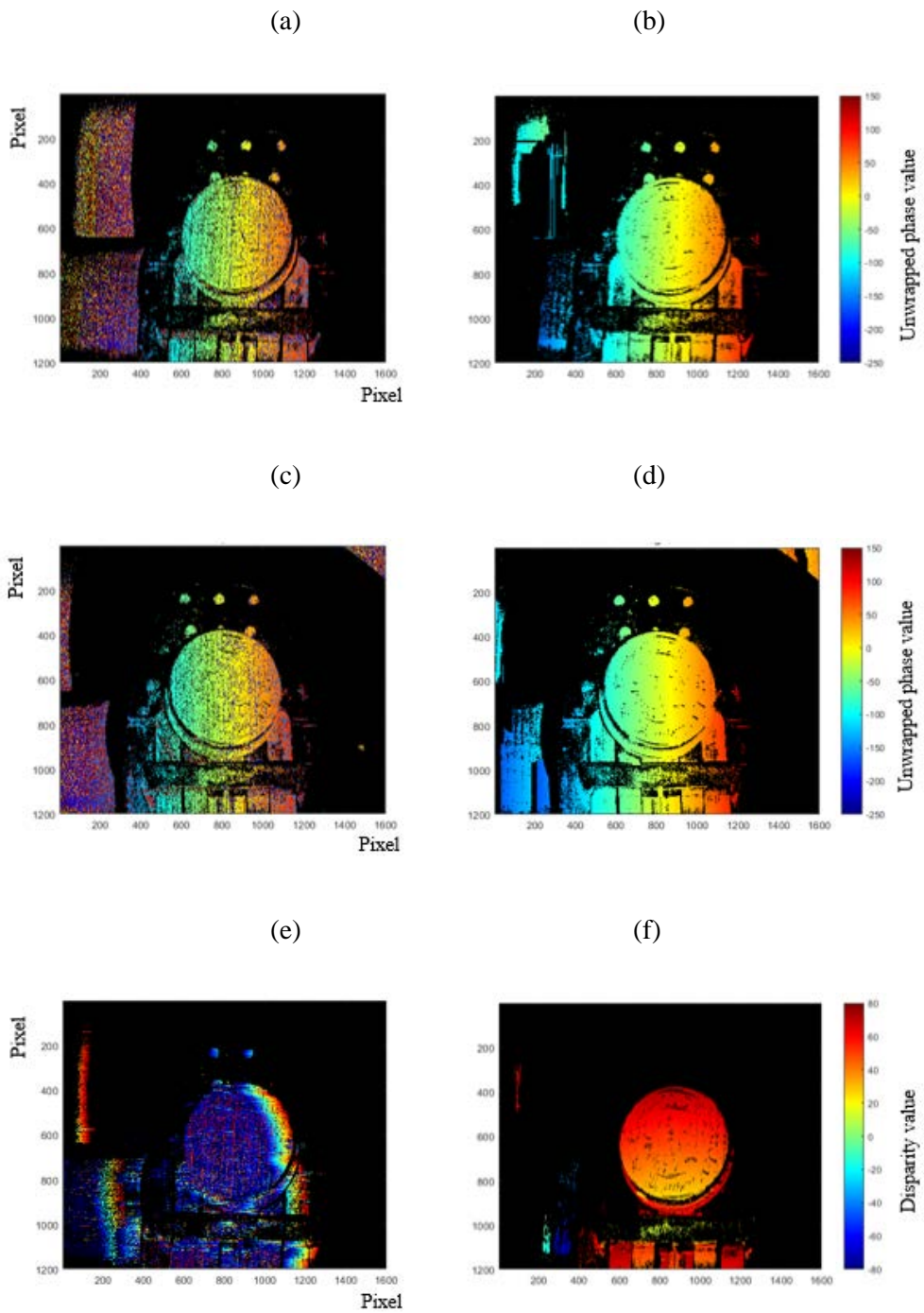


Figure 5-3. (a-b) Left unwrapped phase maps, (c-d) right unwrapped phase maps, and (e-f) disparity maps for an aluminum tin cover; (a, c, e) without error correction and (b, d, f) with error correction applied

5.1.3. Multi-material object: electrical connector

An electrical connector was tested for scanning as shown in Figure 5-1(c). Because the test object is composed of two different materials, rubber and metallic parts, cameras were disturbed by the uneven surface reflection from the pattern projection.

The results from general unwrapping procedure and the error correction applied procedure are displayed in Figure 5-4. By comparing the disparity maps from each method, the suggested method was found to be effective for eliminating noises due to phase errors. For both left and right unwrapped phase maps, the correction-applied maps in Figure 5-4(b) and (d) are devoid of noises. On the other hand, the maps without the error correction contain noises on the object surfaces as shown in Figure 5-4(a) and (c). Additionally, the boundary between the object and the background is clearer in the unwraps phase maps generated using the error correction than those generated without the error correction.

The disparity maps are generated by using both procedures as shown in Figure 5-4(e) and (f), and showed similar results as the unwrapped phase maps. For both rubber and metallic parts, noises are observed in the map generated without the error correction, while they are eliminated in the error correction applied map. Additionally, background noises are observed more severely in the map without the error correction than the one with the error correction applied.

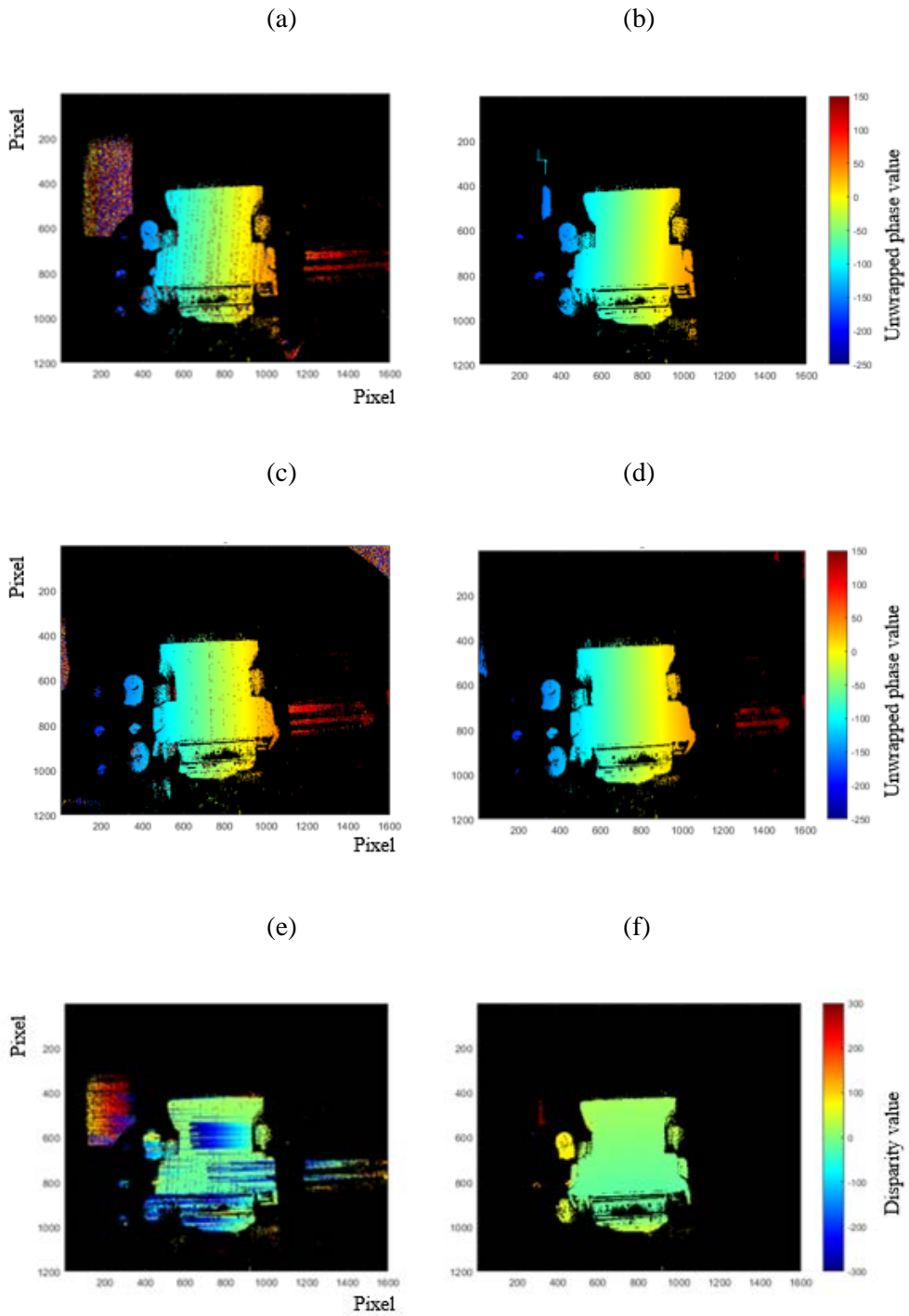


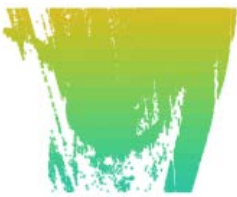



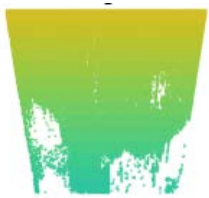



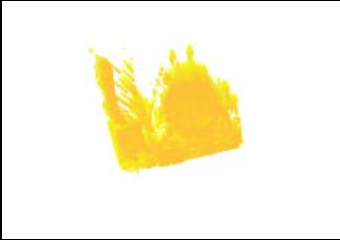



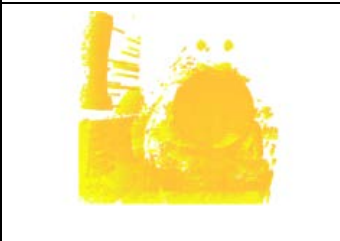





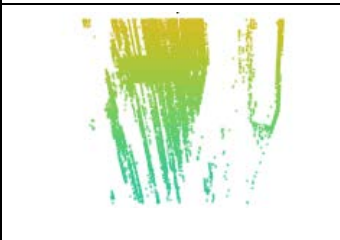

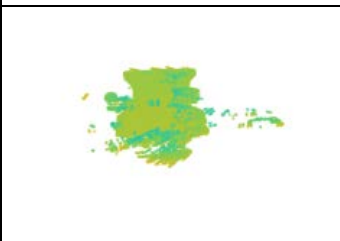

Figure 5-4. (a-b) Left unwrapped phase maps, (c-d) right unwrapped phase maps, and (e-f) disparity maps for an electrical connector; (a, c, e) without error correction and (b, d, f) with error correction applied



5.2. Data Analysis on Results

The three objects that were tested for 3-D scanning were reconstructed into 3-D point clouds, as shown in Table 5-1. As the error correction algorithm was applied to the phase unwrapping procedure, the reconstructed 3-D point clouds clearly showed the original objects at all perspectives. However, it was difficult to distinguish the scanned results without using the error correction because the point clouds were disturbed by noises.

Table 5-1. 3-D reconstructed results for the scanned objects

		Before Error Correction	After Error Correction
Plastic Figurine	Isometric		
	Top		
	Front		
	Right		

Aluminum Tin Cover	Isometric		
	Top		
	Front		
	Right		
Electrical Connector	Isometric		
	Top		
	Front		

	Right		
--	-------	---	--

For the data analysis on the 3-D reconstructed results, all the scanned objects were compared with respect to the inliers and outliers as displayed in Table 5-2. The inliers represent 3-D data points that are located within the acceptable range, while the outliers represent those located outside of the acceptable range. Based on the absolute phase, the acceptable range for each scanned object can be defined. Table 5-2 confirms the performance of the error correction method in that the percentage of inliers is increased for all three objects, as the error correction was applied. The increase in the inliers indicates that an increased number of 3-D points are redirected from the phase error-affected value to the correct value so that they fall into the acceptable range.

Table 5-2. Experimental results comparison

	Before Error Correction		After Error Correction	
	Inlier [%]	Outlier [%]	Inlier [%]	Outlier [%]
Plastic Figurine	25	75	98	2
Aluminum Tin Cover	24	76	98	2
Electrical Connector	65	35	93	7

CHAPTER 6. Conclusion

In this research, the phase error correction was applied to calculate the fringe order, thus generating accurate unwrapped phase maps for a robust 3-D reconstruction. By examining the fringe order of each pixel from the initially captured images, the correction method aptly segregates the correct and incorrect regions. The fringe orders of the separated incorrect regions are then redirected to more reasonable values based on those of the neighboring correct regions. The performance of the error correction method was confirmed as more robust than performing the unwrapping process without it. To verify its performance, a disparity map based on the unwrapped phases from both left and right images was generated. When compared to the disparity map derived from a general phase unwrapping procedure, the map of the suggested method presented the depth of the scanned object, almost devoid of noise due to phase errors. As a result, it generated a disparity map and a 3-D model that clearly displayed the features of the object. Thus, the suggested method allows for robust 3-D scans of objects with varied surface conditions that does not require any surface treatment or modification of the scanning system.

References

- [1] Ricardo R. Garcia and Avidesh Zhkhor, "Consistent stereo-assisted absolute phase unwrapping methods for structured light systems," *IEEE Journal of selected topics in Signal Processing* **6**, 411-424 (2012)
- [2] Shijie Feng, Qian Chen, Chao Zuo, and Anand Asundi, "Fast three-dimensional measurements for dynamic scenes with shiny surfaces," *Optics Communications* **382**, 18-27 (2017)
- [3] David Palousek, Milan Omasta, Daniel Koutny, Josef Bednar, Tomas Koutecky, and Filip Dokoupil, "Effect of matte coating on 3D optical measurement accuracy," *Optical Materials* **40** (2015)
- [4] Hui Lin, Jian Gao, Qing Mei, Yunbo He, Junxiu Liu, and Xingjin Wang, "Adaptive digital fringe projection technique for high dynamic range three-dimensional shape measurement," *Opt. Express* **24**, 7703-7718 (2016)
- [5] Zhaoshuai Qi, Zhao Wang, Junhui Huang, Qi Xue, Jianmin Gao, "Improving the quality of stripes in structured-light three-dimensional profile measurement," *Opt. Eng.* **56**, 031208 (2016)
- [6] Chao Zuo, Lei Huang, Minliang Zhang, Qian Chen and Anand Asundi, "Temporal phase unwrapping algorithms for fringe projection profilometry: a comparative review," *Optics and Lasers in Engineering* **85**, 84-103 (2016)
- [7] Jingang Zhong and Ming Wang, "Phase unwrapping by lookup table method: application to phase map with singular points," *Opt. Eng.* **38**, 2075-2080 (1999)

- [8] Yi Ding, Jiangtao Xi, Yanguang Yu, and Joe Chicharo, "Recovering the absolute phase maps of two fringe patterns with selected frequencies," *Opt. Lett.* **36**, 2518-2520 (2011)
- [9] Yi Ding, Jiangtao Xi, Yanguang Yu, Wenqing Cheng, Shu Wang and Joe F. Chicharo, "Frequency selection in absolute phase maps recovery with two frequency projection fringes," *Opt. Express* **20**, 13238-13251 (2012)
- [10] Yi Ding, Jiangtao Xi, Yanguang Yu, and Fuqin Deng, "Absolute phase recovery of three fringe patterns with selected spatial frequencies," *Optics and Lasers in Engineering* **70**, 18-25 (2015)
- [11] Song Zhang and Shing-Tung Yau, "Generic nonsinusoidal phase error correction for three-dimensional shape measurement using a digital video projector," *Appl. Opt.* **46**, 36-43 (2007)
- [12] Song Zhang, "Recent progresses on real-time 3D shape measurement using digital fringe projection techniques," *Optics and Lasers in Engineering* **48**, 149-158 (2010)
- [13] Hua Du and Zhaoyang Wang, "Three-dimensional shape measurement with an arbitrarily arranged fringe projection profilometry system," *Opt. Lett.* **32**, 2438-2440 (2007)
- [14] Song Zhang and Shing-Tung Yau, "High-resolution, real-time 3D absolute coordinate measurement based on a phase-shifting method," *Opt. Express* **14**, 2644-2649 (2006)
- [15] Peisen S. Huang and Song Zhang, "Fast three-step phase-shifting algorithm," *Appl. Opt.* **45**, 5086-5091 (2006)

- [16] Xianyu Su and Wenjing Chen, "Reliability-guided phase unwrapping algorithm: a review," *Optics and Lasers in Engineering* 42, 245-261 (2004)
- [17] Hong Zhang, Michael J. Lalor, and David R. Burton, "Spatiotemporal phase unwrapping for the measurement of discontinuous objects in dynamic fringe-projection phase-shifting profilometry," *Appl. Opt.* **38**, 3534-3541 (1999)
- [18] Shijie Feng, Qian Chen, Chao Zuo, and Anand Asundi, "Fast three-dimensional measurements for dynamic scenes with shiny surfaces," *Optics Communications* **382**, 18-27 (2017)
- [19] *Handbook of Photoelectric Sensing*. Minneapolis, MN: Banner Engineering, (1993)
- [20] Nordmann, Arne. "File:Epipolar Geometry.svg." File:Cholesterol (chemical Structure).svg - Wikimedia Commons. January 10, 2008. Accessed July 19, 2018.
https://commons.wikimedia.org/wiki/File:Epipolar_geometry.svg.
- [21] Gerig, Guido. "Image Rectification (Stereo)." March 20, 2012. Accessed July 19, 2018. <http://www.sci.utah.edu/~gerig/CS6320-S2012/Materials/CS6320-CV-F2012-Rectification.pdf>.
- [22] "Basics of Computational Stereo Vision." Morphological Image Processing. Accessed July 19, 2018.
<https://www.cs.auckland.ac.nz/courses/compsci773s1t/lectures/773-GG/topCS773.htm>.

[23] Fitzpatrick, Richard. "Law of Reflection." Determination of Metacentric Height. July 14, 2007. Accessed July 19, 2018.
<http://farside.ph.utexas.edu/teaching/3021/lectures/node127.html>.

초 록

본 논문에서는 3차원 스캔 시, 고주파 패턴을 이용하는 상황에도 강건하게 펼친 위상을 획득할 수 있는 방법을 제시하여, 스캔 과정 전체의 견실성을 높이고자 한다. 기존의 3차원 스캐닝 시스템은 프로젝터를 이용하여 고유한 위상 신호를 전달하고, 서로 다른 관점에서 물체를 바라보는 두 개의 카메라를 통해 패턴이 투사된 물체 표면을 촬영한다. 촬영한 영상들을 통해 접힌 위상을 획득하고, 패턴 정보에 맞춰진 특수한 위상 펼침 방법을 통해 펼친 위상을 획득 후, 펼쳐진 위상 및 미리 획득해둔 카메라 파라미터를 통해 3차원 점군을 획득한다. 그러나 지금까지 연구되어 왔던 위상 펼침 알고리즘은 이론적으로는 정확한 값을 가지지만, 실제로는 오류가 포함되어 있는 접힌 위상을 사용하기 때문에, 잘못된 프린지 수를 획득하는 경우가 있다. 특히, 물체의 표면 특성 및 단차가 있는 지점, 그리고 고주파 패턴을 사용하는 경우 등에 대해 오차가 늘어나는 경향을 보인다. 본 논문에서는 잘못 획득되는 프린지 수를 시공간 정보를 동시에 활용하여 정확한 값으로 변경함으로써 펼친 위상에서의 오류를 수정했다. 왼쪽과 오른쪽 카메라에서 획득한 두 영상 모두에 대해 오류 보정이 이루어지면, 보정된 영상을 활용하여 계산을 통해 3차원 모델로 재건된다. 제안된 방법은 다양한 표면 성질을 가진 물체들도 3차원 스캐닝이 가능하다. 그러므로, 스캔하고자 하는 대상에 맞추어서 스캐너 셋업 및 알고리즘을 수정해야하는 과정이 필요하지 않게 된다. 또한, 스캔 대상도 스캐닝에 적합한 상태로 만들기 위한 어떠한

표면 처리도 필요하지 않다. 논문에서 제시한 오류 보정 알고리즘을 사용하면, 위상 오류로 인한 영상 노이즈를 효과적으로 조절하여 견실한 3차원 스캐닝 결과를 얻을 수 있다.